

[CH]

Sediment-laden gravity currents with reversing buoyancy

R. Stephen J. Sparks^a, Roger T. Bonnecaze^b, Herbert E. Huppert^b,
John R. Lister^b, Mark A. Hallworth^b, Heidy Mader^c and Jeremy Phillips^a

^a Department of Geology, University of Bristol, Bristol BS8 1RJ, UK

^b Institute of Theoretical Geophysics, Department of Applied Mathematics and Theoretical Physics, University of Cambridge,
Silver Street, Cambridge CB3 9EW, UK

^c Institute of Environmental and Biological Sciences, Lancaster University, Lancaster LA1 4YQ, UK

Received June 11, 1992; revision accepted November 5, 1992

ABSTRACT

There are many natural occurrences of sediment-laden gravity currents in which the density of the interstitial fluid is less than that of the ambient fluid, although the bulk density of the current is greater. Such currents are driven by the excess density of suspended particles. However, after sufficient particles have sedimented, the current will become buoyant, cease its lateral motion and ascend to form a plume. Examples of such currents include brackish underflows in deltas, turbidity currents and pyroclastic flows. Experimental studies are described which show that, due to sedimentation, sediment-laden gravity currents decelerate more rapidly than saline currents of the same density. There is little difference in the experiments between a sediment-laden current with neutrally buoyant interstitial fluid and one with buoyant interstitial fluid until sufficient sediment has been lost to cause the latter kind of current to lift-off. A marked deceleration is then observed and a plume is generated, with lift-off occurring along the length of the current. The resulting buoyant plume then generates a gravity current below the upper surface of the fluid in the tank. The deposit from a current with buoyant fluid shows a fairly abrupt decrease in thickness beyond the lift-off distance and has a flatter profile than that from a simple sediment current. A theoretical model is presented, which is based on the two-layer shallow-water equations and incorporates a model of the sedimentation in which particles are assumed to be uniformly suspended by the turbulence of the current. The model shows good agreement with the observed lengths of the experimental currents as a function of time and predicts the lift-off distance reasonably well. These processes have implications for the behaviour of turbidity currents, the interpretation of turbidites, mixing processes in the oceans and the lift-off of pyroclastic flows.

1. Introduction

Gravity currents are one of the principal mechanisms of sediment transport. Examples include turbidity currents in oceans and lakes [1–3], dense underflows where sediment-laden rivers enter the sea [4], dust storms in deserts [1] and pyroclastic flows generated by explosive eruptions [5]. Theoretical and experimental studies [6–10] of sediment-laden gravity currents have emphasized the essential role played by the density

difference between the gravity current and the ambient fluid. Theoretical studies have also paid particular attention to the phenomenon of auto-suspension, whereby a current on a slope maintains or increases its density by erosion of sediment [8–10]. Rather less attention has been paid to the theoretical analysis of turbidity currents in the depositional regime, which is perhaps the situation of most significance for the interpretation of the geological record. Positional models are largely based on experimental studies by Middleton [11] and treat sedimentation as collapse of an unsupported sediment dispersion [12]. No work has hitherto been published on the overall interaction between flow and sedimentation.

In many natural situations the interstitial fluid of a sediment-laden gravity current can have a

Correspondence to: H.E. Huppert, Institute of Theoretical Geophysics, Department of Applied Mathematics and Theoretical Physics, University of Cambridge, Silver Street, Cambridge CB3 9EW, UK.

smaller density than the ambient fluid even though the bulk density of the current is larger. For example, although the oceans are stably stratified, turbidity currents often transport warmer buoyant water into deep basins from continental shelf regions above the thermocline. Similarly, underflows generated in deltaic environments by rivers can contain water which is less saline than the oceans [4]. Air entrained by pyroclastic flows is heated by the particles and expands greatly with a consequent decrease in density [5,13,14]. The effects of the buoyant interstitial fluid on such currents is the focus of this paper.

Observations of pyroclastic flows, such as those generated at Mt. St. Helens in 1980 [14] and Mt. Redoubt in Alaska in 1990 [15], have recognized the phenomenon of lofting, in which the flow lifts off the ground to form a plume, which is often fed by the entire area covered by the flow. This spectacular phenomenon may be due both to sediment sorting processes within the flow and to heating of cold air entrained into the flow, which causes the mixture of hot air and fine suspended particles to become buoyant relative to the overlying atmosphere. Motivated by these observations, Carey et al. [16] investigated phenomena associated with small-scale laboratory turbidity currents containing fresh water as they spread along the floor of a tank containing salty water. These currents spread out radially from a point source and then lofted from a ring of vigorous plumes generated at the flow front, which transported fine sediment to the top of the experimental tank. A feature of these experiments was that the flow front remained at a fixed position for constant values of the input flow rate, sediment concentration and grain size.

The lift-off phenomenon can occur in many other geological and oceanographic situations. In the stably stratified oceans, turbidity currents will transport more oxygenated warmer surface waters into deep ocean basins [17]. In low latitudes, lift-off will typically occur when the concentration of sediment in the current is 3–4 kg m⁻³. Upward mixing of oxygenated water and fine sediment in deeper water environments may lead to significant temporary changes in nutrient levels and biota and could contribute to the formation of the nepheloid layer in the deep oceans. Lift-off should influence the character of the turbidite

and the dispersal of fine sediment components. Buoyant lift-off should also have a significant impact on sedimentation patterns at delta fronts and in estuaries where the process will limit the movement of brackish underflows.

Aspects of the local fluid mechanical processes associated with lift-off have been studied in a number of theoretical and experimental investigations. The behaviour of a layer of suspended fine particles in fresh water below a layer of salty or sugary water in which the bulk density of the suspension exceeds that of the overlying fluid, but in which the density of the interstitial fluid (water) is less than that of the upper layer was investigated by Huppert et al. [18]. As the sediment settled and segregated, buoyant fluid was released from the interface between the two layers causing convection and mixing of the finer fractions of the sediment throughout the upper layer. Kerr [19] extended this work by considering the effects of a concentration gradient in the upper layer, a condition that is relevant to many oceanographic situations. Sedimentation in a thermally convecting suspension heated from below was considered by Koyaguchi et al. [20], who observed well-defined convective overturn events, which occurred when the warmer fluid in the suspension layer became buoyant relative to the colder overlying fluid and ascended while lofting some of the sediment. Quantitative theoretical models were presented for the sedimentation from the suspension containing buoyant interstitial fluid in these cases [18–21] and the theoretical predictions agreed well with the experimental observations.

In this paper we present an experimental and theoretical study of sediment-laden gravity currents containing buoyant interstitial fluid. We compare the behaviour of: (i) simple saline currents, (ii) simple sediment-laden currents and (iii) sediment-laden currents with buoyant fluid. Ex-

TABLE 1
Particle-size analysis of alumina powder

Size	Wt. %
> 71 μm	0.03
63–71 μm	82.48
53–63 μm	12.11
< 53 μm	5.39

TABLE 2

Experimental conditions. The gravity currents had initial bulk density ρ_c and interstitial fluid density ρ_i ; the ambient fluid density was ρ_a . The initial volume fraction of a current is ϕ_0 and $\gamma = (\rho_a - \rho_i)/[(\rho_p - \rho_i)\phi_0]$. The values of the density differences for Run J are based on the density of $\rho_a = 1011 \text{ kg m}^{-3}$ at the base of the stratified tank

Run	Ambient Fluid	Gravity Current	ρ_c (kg m^{-3})	$\rho_c - \rho_a$ (kg m^{-3})	$\rho_a - \rho_i$ (kg m^{-3})	ϕ_0	γ (%)
A	Fresh water	7 wt.% saline solution	1050	50.0	—	—	—
B	Fresh water	Sediment in fresh water	1050	50.0	0	0.017	0
C	1.3 wt.% saline solution	Sediment in fresh water	1050	50.0	10.0	0.020	0
D	Fresh water	Sediment in 2.1 wt.% aqueous methanol	1041	41.0	4.7	0.015	10
E	Fresh water	Sediment in 4.8 wt.% aqueous methanol	1037	37.0	9.4	0.015	20
F	Fresh water	Sediment in 12.4 wt.% aqueous methanol	1048	48.0	21.1	0.023	30
G	Fresh water	Sediment in 17.3 wt.% aqueous methanol	1041	43.0	28.1	0.023	40
H	Fresh water	Sediment in 36.1 wt.% aqueous methanol	1036	38.0	54.2	0.030	60
I	Fresh water	Sediment in 56.0 wt.% aqueous methanol	1023	23.0	93.6	0.038	80
J	Gradient 0.45–1.5 wt.% saline solution	Sediment in fresh water	1034	23.0	24.0	0.016	67
K	1.3 wt.% saline solution	Sediment in fresh water	1034	24.0	10.0	0.012	28
L	1.3 wt.% saline solution	Sediment in fresh water	1043	33.0	10.0	0.015	22
M	1.3 wt.% saline solution	Sediment in fresh water	1067	57.0	10.0	0.023	15
N	1.3 wt.% saline solution	Sediment in fresh water	1088	78.0	10.0	0.030	11
O	1.3 wt.% saline solution	Sediment in fresh water	1103	93.0	10.0	0.035	10

periments in a laboratory tank are described which were carried out in either uniform or stratified environments. We present a new theoretical model for sedimenting gravity currents and apply the model to predict the rate of propagation of sediment-laden gravity currents, the distance at which lofting takes place and the distribution of the final deposit. In the last section we discuss the implications of these processes for the behaviour of turbidity currents, the interpretation of turbidites, mixing processes in the oceans and the lift-off of pyroclastic flows.

2. Experimental studies

The experimental apparatus was a simple rectangular tank 6 m long, 100 cm high and 20 cm wide, which was filled to a depth of 40 cm. A sluice gate was positioned 20 cm from one end. The experiments used the lock-exchange technique in which a fixed volume of dense fluid was released by rapidly lifting the sluice gate [1]. The gravity currents were filmed and photographed to record the variations in their length and height. For the sediment-laden gravity currents the mass of sediment deposited per unit area was determined by placing a perspex tube on the floor of the tank and siphoning the sediment from the circular area enclosed by the tube. Alumina particles with a mean diameter of $66.5 \mu\text{m}$ (Table 1) and a density of 3985 kg m^{-3} were used. Settling-tube experiments with fresh water, salty water and sugary water established that there were no flocculation effects for the particle sizes used in the experiments, but 0.15 wt.% of the anti-flocculent Calgon was nevertheless added as a precaution. Blue dye was added to the mixture to provide a qualitative indication of the extent of dilution by mixing processes in the current. The experiments were all conducted at room temperature ($15\text{--}20^\circ\text{C}$).

The behaviour of a gravity current formed by sudden release of a fixed volume of dense sediment-free fluid is well established [1]. The gravity current consists of a billowing head, followed by the body of the current with a mixing layer above the current, which is shed from the head as sketched in Fig. 1. The velocity of the head is approximately constant for a distance of about 200 cm, which is approximately ten times the lock



Fig. 1. The anatomy of a simple gravity current.

length in these experiments. Beyond this distance the increase in the length is proportional to $t^{2/3}$ (the velocity decreases in proportion to $t^{-1/3}$) as long as the Reynolds number remains sufficiently high that viscous effects can be ignored. Figure 2 shows the results of a pure saline gravity current (Run A in Table 2) which confirms the results of previous studies. The Reynolds number of the current, evaluated at the front, decreased from 3×10^4 to 9×10^3 , which indicates that the experiment was always in the fully turbulent inertial regime.

We compared the behaviour of three different currents with identical density contrasts between the initial mixtures and the ambient fluid. The details of the conditions for each experiment reported here are listed in Table 2. Run B consisted of alumina particles suspended in fresh water and released into fresh water. Run C consisted of alumina particles suspended in fresh water and released into salty water (1.3 wt.% concentration). The variations of distance with time of the three currents A, B and C are compared in Fig. 3. Over the first 1.5 m the three

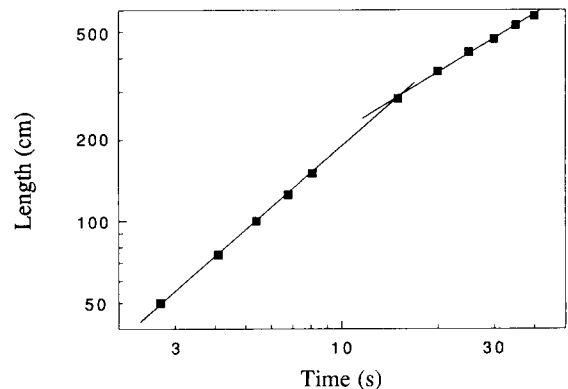


Fig. 2. Experimental data for the length of a saline gravity current (Run A in Table 2) showing the initial slumping phase in which the length is proportional to t and the subsequent flow in which the length travelled is proportional to $t^{2/3}$. Regression lines through the data yield values of the exponent n of 1 and 0.71, in reasonable agreement with theoretical values of 1 and 0.66.

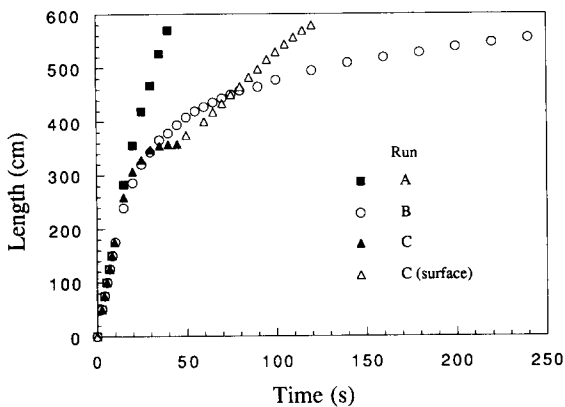


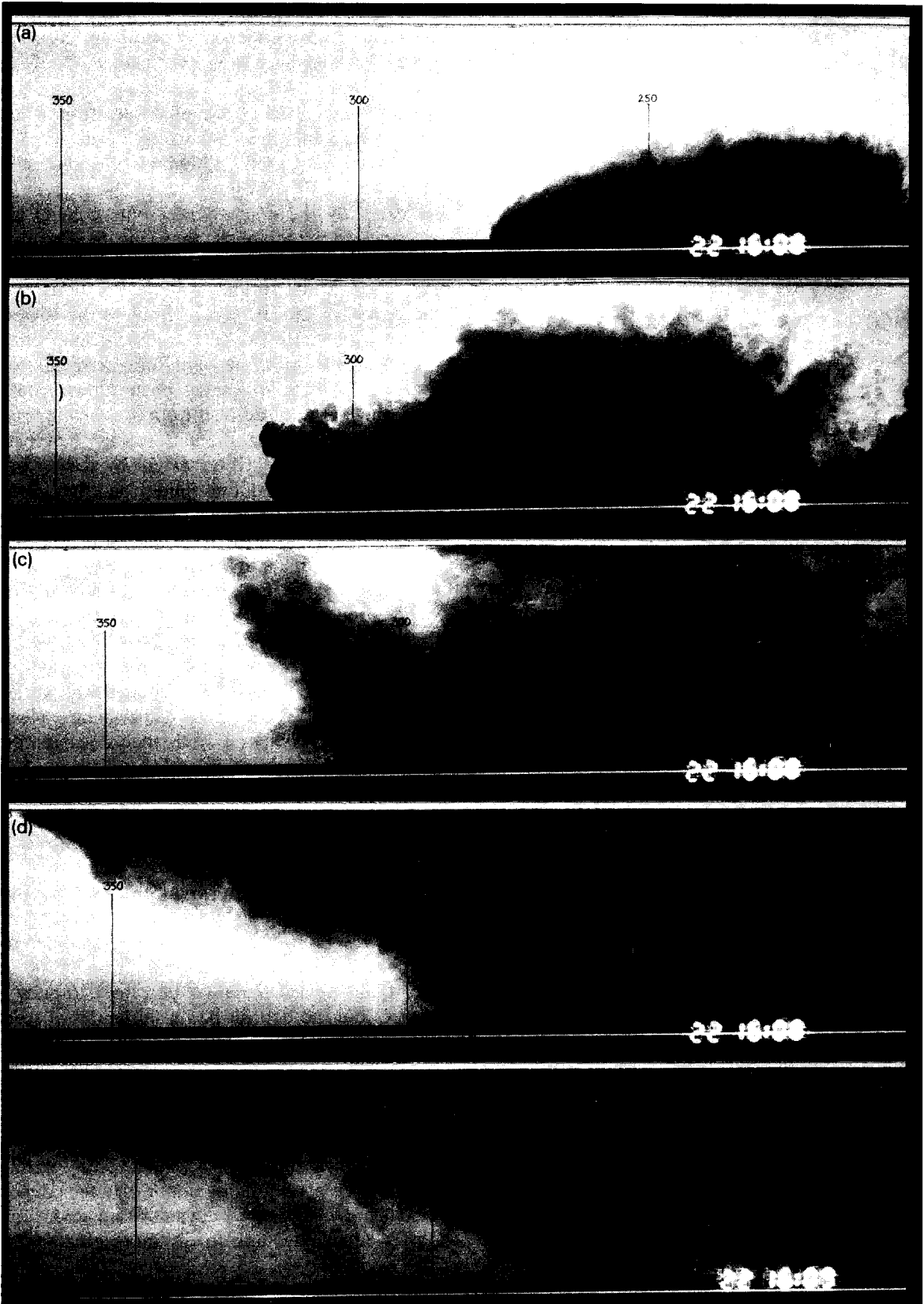
Fig. 3. (a) Distance versus time data for three gravity currents with identical initial values of reduced gravity. Run A is a saline current, Run B is a sediment-laden gravity current with neutrally buoyant interstitial fluid and Run C is a sediment-laden gravity current with buoyant interstitial fluid. The open triangles show the lateral motion of the gravity current formed below the upper surface of the tank by the lofted fluid. (b) Distance versus time data for the first 150 cm of propagation for Runs A–C. In these initial stages, little sediment has been deposited in Runs B and C, and the three currents propagate at almost the same rate.

currents are almost indistinguishable. However, beyond 2 m the length of the sediment-laden currents increases less rapidly (Fig. 3) compared with that of the saline current. The sediment-laden current with neutrally buoyant fluid (Run B) propagated to the end of the tank, but most of the sediment was deposited within the first 3 m. The alumina powder has a narrow size cut but contains minor amounts of fine particles (Table 1) and the slow motion towards the end of run B is attributed to the fines remaining in suspension. In this run the Reynolds number fell below 1000 at a distance of 4.3 m and had decreased to 300 by the end of the tank, and therefore viscous effects had begun to influence the flow.

The current containing buoyant fluid (Run C) initially behaved like that of Run B to a distance of over 3 m (Fig. 4a). Beyond this distance the current decelerated much more rapidly (as seen in Fig. 3) and the first visible effects of buoyant interstitial fluid became evident (Fig. 4b). After about 21 s, parts of the dilute layer shed by mixing behind the flow head were observed to rise off the current, which indicates that the upper parts had become weakly buoyant. The upper surface of the current at a distance of 2.5

m ascended with increasing vigour, which is interpreted as a consequence of sediment loss and increasing buoyancy (Fig. 5). The front of the flow began to decelerate significantly after about 33 s and ascended at a similar rate (Fig. 4 and 5b). By 40 s and at a distance of 3.6 m, the flow head was completely stationary and the more concentrated fluid in the head of the current (as indicated by the much darker blue colour) had ascended to the top of the tank (Fig. 5). This fluid formed a gravity current under the free surface of the water, which spread in both directions from the region of lift-off. Figure 3 shows the velocity of the surface current in the downstream direction from the lock. Buoyant fluid derived from the head had a noticeably deeper blue colour than buoyant fluid derived from the mixing layer, which indicates that the latter fluid had been diluted to a much greater extent by mixing processes. The more dilute fluid from the mixing layer spread slowly below the surface current formed by lift-off of the head and formed a thick stratified region about 20 cm thick (Fig. 4e). Fine particles that were carried by the lofted fluid sedimented out over approximately the next 10 min. Behaviour similar to the above was observed for a series of experiments similar to Run C in which the initial load of sediment was varied. Measurements from these experiments (Runs K–O) will be compared with theoretical predictions in the following section.

The mass of deposited sediment per unit area decreased with distance in both Runs B and C (Fig. 6a). The pattern of sedimentation, however, was somewhat different. It is apparent that the simple sediment current spread the sediment over a greater length and that, up to the distance of lift-off, the buoyant current (Run C) sedimented a greater proportion of its load. Beyond 360 cm the sediment accumulation decreased rapidly in Run C and the deposit had a fairly abrupt front. The difference in deposit geometry is attributed to buoyant lift-off which slowed the current and allowed much of the sediment to be deposited. Additional sediment was added to the deposit as the buoyant cloud ascended and was then spread up and down the tank by the resulting surface gravity current. A small amount of fine sediment was taken up by the buoyant cloud and transported along the tank to distances greater than



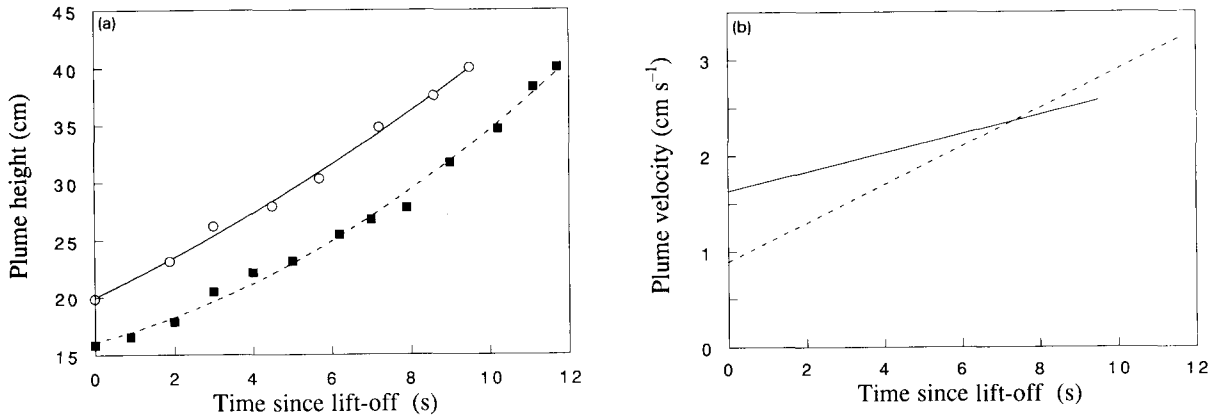


Fig. 5. (a) The height of the plume rising above the sediment-laden current in Run C is shown against time at two fixed positions. Time is evaluated from when upward motion of the plume was first noticed. The data were taken at the lift-off distance of 325 cm (■ and dashed line) and at 250 cm (○ and solid line). The curves are best-fit quadratic polynomials. (b) The velocity of the plume at lift-off versus time for the same two fixed positions determined by differentiating the best-fit quadratic polynomials in (a).

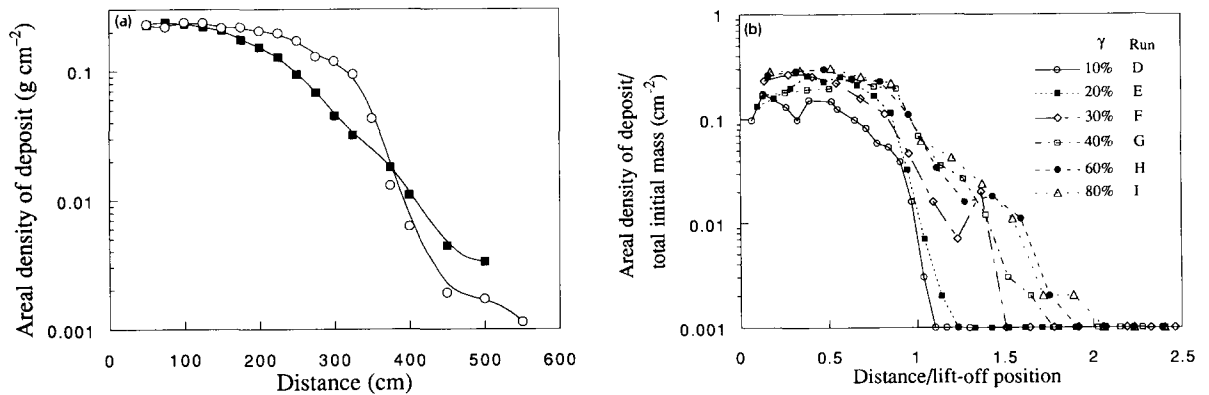


Fig. 6. (a) The accumulation of sediment in g cm⁻² plotted against distance for Run B (■) and Run C (○) showing proximal maxima in sediment accumulation and general decrease of deposit thickness with distance. (b) The mass accumulation of sediment divided by the total initial mass as a function of normalized distance for Runs D–I. Note that greater amounts of sediment are transported beyond the lift-off position for the larger values of γ , which is the approximate proportion of particles carried up by the plume.

360 cm where lift-off occurred, which produced a minor accumulation of sediment beyond the lift-off distance.

At the stage of lift-off Run C contained only a small suspended load which could be entrained in the plume and transported up and down the tank by the surface current. Hence, we investigated

the effect of varying the proportion of sediment still in suspension at lift-off. An approximate measure of this load is the proportion, γ , of the original sediment mass required to achieve a bulk density equal to the ambient, and this was varied from 10 to 80% in Runs D–I (Table 2). The broad behaviour of these experiments was similar

Fig. 4. A sequence of photographs of a typical sediment-laden gravity current with buoyant interstitial fluid in which lift-off occurs. The propagation of the current, the rise of the interstitial fluid to the free surface and the subsequent spread along the free surface are described in the text.

to that described for Run C. However, two sedimentation patterns are apparent, as may be seen in Fig. 6b where the areal density of mass deposited divided by the total initial mass of sediment is plotted against the distance normalized by the length of the current at lift-off. For the lesser loads of suspended sediment (small γ), the patterns are similar to those observed for Run C, with minor sedimentation beyond the lift-off distance. For the greater suspended loads (Runs G–I), significant amounts of sediment were deposited well beyond the point of lift-off. Sediment was also transported upstream of the point of lift-off by the gravity current on the surface that arose from the plume which led to flatter profiles of the normalized density of deposit. The difference between Runs D–E and Runs G–I is interpreted as being a consequence of the weaker plumes in the former set of experiments which were unable to lift much sediment into the surface gravity current.

All these runs were carried out in a homogeneous environment, although some reconnaissance experiments, of which Run J is an example (Table 2), were carried out in a stratified tank. A linearly stratified saline environment was achieved using the standard double-bucket technique, with a saline concentration of 1.5% ($\rho_a = 1011 \text{ kg m}^{-3}$) at the base of the tank and 0.45% ($\rho_a = 1003 \text{ kg m}^{-3}$) at the top. The current was composed of dense particles suspended in a solution of methanol, ethanol and water ($\rho_i = 987 \text{ kg m}^{-3}$). The current in Run J initially behaved in a similar way to Run C, propagating like a dense current (Fig. 7a) until sufficient particles had settled out, at which point the head began rising as a buoyant plume (Fig. 7b). The gravity current generated by lofting of fluid from the head of the bottom current ran just below the upper surface of the stratified fluid (Fig. 7c and d). However, fluid lofting from the more dilute mixing layer intruded at an intermediate level as a separate gravity current (Fig. 7d). Clear fluid separated the two gravity currents generated by buoyant lift-off. Thus, the single basal current produced two intrusions in the stratified tank, a more vigorous, low-density intrusion formed by lofting of the flow head, and a weaker, medium-density intrusion by lofting of the mixing layer or body of the current.

3. Theory

The experiments on sediment-driven gravity currents can be modelled well using a hydraulic approach, the basic elements of which are described in [22]. The initial collapse of the gravity current is a complex three-dimensional unsteady flow. However, once the current has spread sufficiently that its length is significantly greater than its height and that the height along the gravity current is slowly varying, it is a good approximation to ignore vertical accelerations in the fluid and assume a hydrostatic pressure distribution at any horizontal position x and time t in both the ambient and sediment-laden fluids. As long as viscous forces are negligible, it can also be assumed that the horizontal velocities, $u_1(x,t)$ and $u_2(x,t)$ in the lower gravity-current layer and the upper ambient layer, respectively, are uniform across the depths of each layer, $h_1(x,t)$ and $h_2(x,t)$, as depicted in Fig. 8. The effects of mixing between the two layers are assumed to be negligible.

Applying these considerations, we derive the two-layer inviscid shallow-water equations in non-dimensional form, which are the conservation of mass in each of the two layers

$$\frac{\partial h_1}{\partial t} + \frac{\partial}{\partial x}(u_1 h_1) = 0 \quad (1a)$$

$$\frac{\partial h_2}{\partial t} + \frac{\partial}{\partial x}(u_2 h_2) = 0 \quad (1b)$$

and the combined conservation of momentum of the two fluid layers

$$\begin{aligned} \frac{\partial}{\partial t}(u_1 h_1) + h_2 \frac{\partial}{\partial x} \left(\frac{1}{2}(\phi - \gamma)h_1^2 + u_1^2 h_1 \right) \\ - h_1 \frac{\partial}{\partial x} (u_2^2 h_2) = 0 \end{aligned} \quad (2)$$

where $\phi(x,t)$ is the ratio of the volume fraction of sediment to its initial concentration ϕ_0 . The approximate proportion of particles lifted by the plume, γ , is given by $\gamma = (\rho_a - \rho_i) / [(\rho_p - \rho_i)\phi_0]$, where ρ_a , ρ_i and ρ_p are the densities of the ambient fluid, the interstitial fluid and the solid particles, respectively. The parameter γ may also be interpreted as the scaled volume fraction at which the current is locally neutrally buoyant. The various terms in eq. (2) represent the rate of

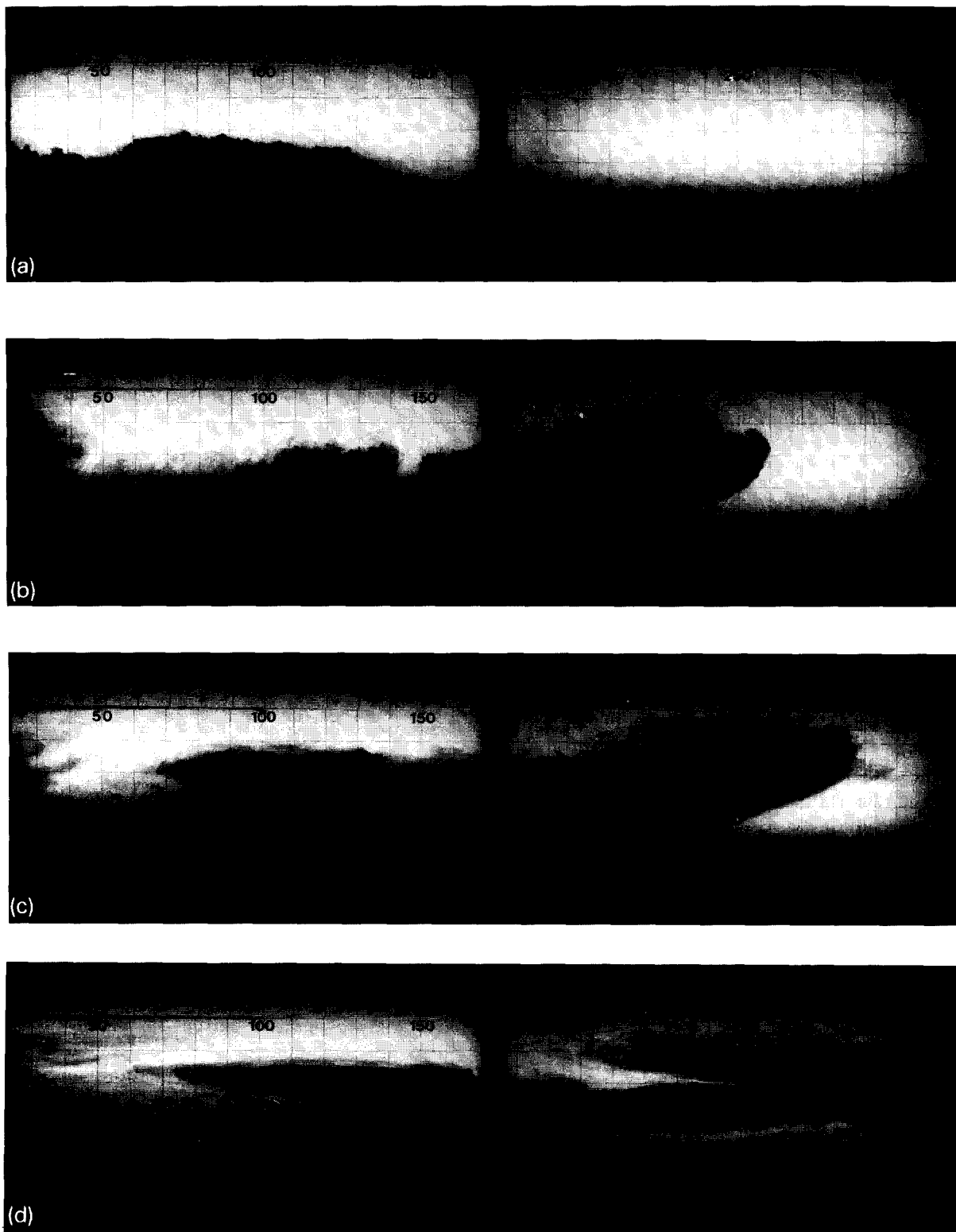


Fig. 7. A sequence of photographs of a buoyancy-reversing gravity current in a stratified environment (Run J). It propagates initially as a dense current (a) until sufficient particles have settled out that the head of the current begins to rise like a buoyant plume (b) to its level of neutral bouoyancy just below the top of the tank (c) and subsequently (d) spreads laterally. Meanwhile, the dilute mixing layer rises to an intermediate height and spreads laterally (c), which results in two intrusions or a double-anvil structure (d) from a single event.

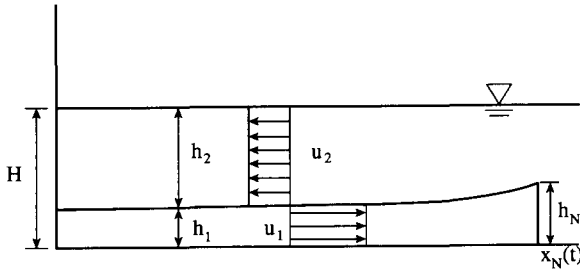


Fig. 8. Schematic representation of a two-dimensional gravity current of initial bulk density ρ_c propagating into an environment of lesser density ρ_a and depth H . Over the length $0 < x < x_n(t)$ the flow is modelled as a two-layer hydraulic flow in which the layer depths and velocities are as shown.

change of momentum in layer 1 due to the buoyancy forces and the advection of momentum in layers 1 and 2. In (1) and (2) the length and time variables are non-dimensionalised by H and $\sqrt{H/g'}$, where H is the fixed total depth of the two fluid layers and $g' = g(\rho_p - \rho_i)\phi_0/\rho_a$ is the reduced gravity due to the density of the particles.

The particle concentration varies throughout the length of the current due to advection by the current and to the settling out of the sediment. We assume that the sediment concentration is vertically uniform due to turbulent mixing, but that the flow is not sufficiently vigorous to re-entrain settled particles. We also ignore concentration gradients due to mixing processes at the flow head. With these assumptions, the non-dimensional equation of particle conservation is

$$\frac{\partial \phi}{\partial t} + u_1 \frac{\partial \phi}{\partial x} = -\beta \frac{\phi}{h_1} \quad (3)$$

with the non-dimensional coefficient for the rate of sedimentation, β , given by

$$\beta = \frac{v_s}{\sqrt{g'H}} \quad (4)$$

where v_s is the Stokes settling velocity of an isolated particle, which is the appropriate velocity because the Reynolds number of the particles and their concentration is small. The rate of sedimentation represented by the right-hand side of eq. (3) assumes that monodisperse particles settle out through the thin viscous sublayer at the bottom of the current. This approach has been

used successfully in several studies of sedimentation from turbulent suspensions [23–26].

The boundary conditions for the equations are no flow at the end wall $x = 0$

$$u_1 = u_2 = 0 \quad (5a,b)$$

and the previously determined experimental relationship [27] between the velocity and the pressure head at the front of the current $x = x_n(t)$, which is given non-dimensionally by

$$u_1 = 1.19\sqrt{(\phi - \gamma)h_1} \quad (0 \leq h_n \leq 0.075) \quad (6a)$$

$$u_1 = 0.5h_1^{-1/3}\sqrt{(\phi - \gamma)h_1} \quad (0.075 \leq h_n \leq 1) \quad (6b)$$

where h_n is the height of the current at the front. The head of a gravity current is in fact a zone of rolling and billowing three-dimensional turbulent motion, and eq. (6) is an effective lumped boundary condition, which gives rise to the abrupt front of the current in Fig. 8. Finally, we note that since the total depth of the two fluid layers is constant

$$h_1 + h_2 = 1 \quad (7)$$

and because there is no flow at the end wall, the velocities in the two layers are everywhere related by the zero-flux condition

$$u_1(x, t)h_1(x, t) + u_2(x, t)h_2(x, t) = 0 \quad (8)$$

which may be deduced from eq. (1). Thus we need only solve equations (1a), (2) and (3).

The equations and boundary conditions described constrain the resulting behaviour of the sediment-laden gravity current depending upon the initial conditions, the settling parameter β and the interstitial fluid parameter γ . Here we concentrate on the results for the case of buoyant interstitial fluid laden with sufficient dense particles that the gravity current is initially denser than the ambient fluid. A more detailed derivation and discussion of the equations and their numerical solutions is presented by Bonnecaze et al. [28]. One result of this study was that the above two-layer shallow-water equations should be used to accurately model lock-exchange experiments, such as those discussed earlier; since the depth of the overlying fluid is comparable to the depth of the gravity current, the effects of the

motion of the upper layer strongly influences the flow of the current. However, if the overlying fluid is very deep, as in some geological situations, its effects can be ignored and the single-layer shallow-water equations can be used to model the flow.

When β and γ are zero, the equations have an analytical solution [29,30], in which the length of a current with an initial volume per unit width q of dense fluid is given asymptotically in dimensional form by

$$x_n(t) = C(g'q)^{1/3}t^{2/3} \quad (9)$$

where the constant $C = 1.6$ for the boundary condition in eq. (6). This result is applicable for the motion at the intermediate time which occurs after the “slumping phase” [27] when the overlying fluid plays a significant role, and before the viscous forces dominate the inertial forces in the gravity current.

When $\beta \neq 0$, eq. (1a), (2) and (3) must be solved numerically, and we employed an explicit two-step Lax–Wendroff scheme, which is accurate to second order in both space and time. The equations are transformed to a new spatial variable $y = x/x_n(t)$ so that the spatial computations are confined to the range [0,1]. The velocity of the nose is explicitly determined at each time step and the length of the current is advanced in time with a trapezoidal integrator that is also accurate to second order. The initial conditions of all the numerical currents was zero velocity everywhere and $h(x,0) = 1$ and $x_n(0) = 0.5$, which are the non-dimensional height and length of the fluid behind the lock.

The model involves a degree of approximation because mixing at the flow head leads to entrainment of surrounding fluid and formation of a diluted mixing layer overlying a more concentrated underflow. Some particles will be entrained into this mixing layer and will then sediment back into the main current below. The model ignores this entrainment process and the recycling of particles through the region of the flow head. Comparison of the theory with laboratory results and application to larger scale currents in the natural environment will require these simplifications to be borne in mind.

The numerical solution for the lengths as functions of time for the saline gravity current, the

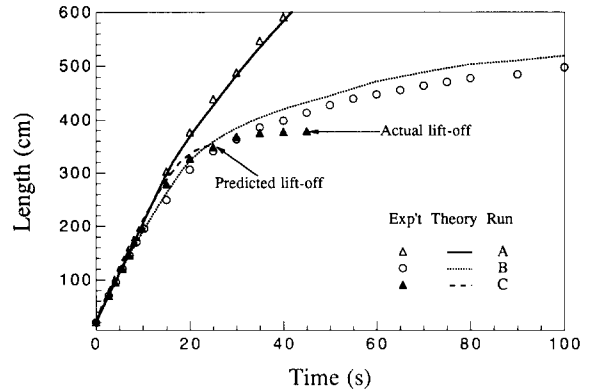


Fig. 9. The experimental observations and theoretical predictions of the length of a simple saline gravity current (Run A), a sediment-laden gravity current (Run B) and a sediment-laden current with buoyant interstitial fluid (Run C).

sediment-laden gravity current, and the sediment-laden gravity current with buoyant interstitial fluid described in section 2 are presented in Fig. 9. The agreement between the predictions and the experiments is seen to be very good for the saline and sediment-laden currents, despite ignoring the mixing in the flow head. The numerical prediction for the sediment-laden current with buoyant interstitial fluid is also very good, up to the point where the numerical curve ends, at which point the head of the model gravity current is neutrally buoyant and is predicted to lift off. Experimentally, the head is observed to lift off somewhat later than predicted. This may be because the buoyant force on the head does not become substantial until more particles have settled, an effect that can be observed in Fig. 4b. The current may thus move a little further as a consequence of its forward momentum. Another possible explanation is that the upward mixing of particles in the flow head would recycle some particles into the flow behind, which results in a slightly lower sedimentation rate than that predicted by eq. (3).

In Figure 10 we compare the numerically and experimentally determined lengths as functions of time for currents with buoyant interstitial fluid, as in Run C, with five different initial loads of particles (Runs K–O). In all cases the early behaviour of the currents is very well described by the theory. However, the time of lift-off is consistently predicted to be 25 s, while the experiments tend to show the lift-off time increasing with the

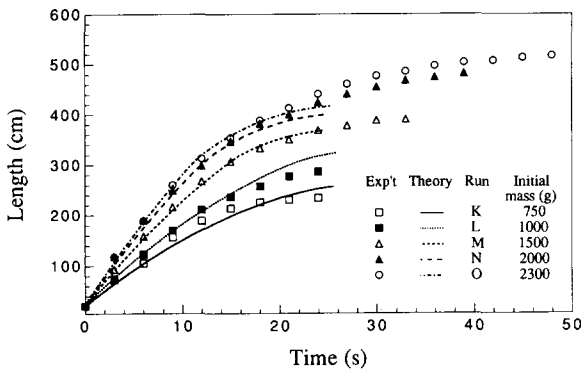


Fig. 10. The experimental observations and theoretical predictions of the length of sediment-laden currents with buoyant interstitial fluid for the different initial loads of sediment in Runs K–O.

initial mass of sediment (Fig. 11). The model overpredicts the lift-off distance for low values of the initial sediment mass and slightly underpredicts it for the larger initial values, and the errors are of order of 20–25%.

The model assumes that the particles are of a single size, whereas the presence of finer particles in the experiments (cf. Table 1) may be important for the currents that must settle out a relatively large fraction of the particles to become buoyant, such as Runs N and O. The finer particles will be retained in suspension longer than average, so that considerably after the release of

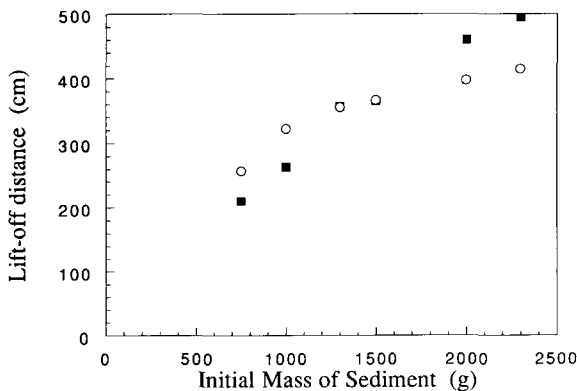


Fig. 11. The experimental observations (■) and theoretical predictions (○) of the lift-off distance of sediment-laden currents with buoyant interstitial fluid for different loads of sediment.

the current, the fluid is denser than expected and hence the lift-off occurs later than predicted. Likewise, larger particles in the initial suspension settle out more rapidly than average, so more particles are lost during the slumping phase than predicted. Thus currents that have to lose fewer particles to become neutrally buoyant, such as Runs K and L, may lift-off sooner than expected. Finally, the recycling of particles through the flow head may play a more important role in the longer currents, resulting in a somewhat lower sedimentation rate.

4. Applications

4.1 Turbidity currents

Turbidity currents are recognised as the main way by which sediment from the continental shelf and shallow-water coastal regions is transported to the deep parts of ocean basins [2,3]. In general, the oceans are stably stratified and water within the uppermost 600 m of the oceans has a lower intrinsic density (σ_T value) than deep water. Water above the thermocline is typically warmer but more saline. Oceanic turbidity currents will therefore transport warmer and intrinsically buoyant water to the depths of the oceans where temperatures are rather uniform (2–4°C). The temperature contrast between shallow and deep ocean water is seasonal, and maximum temperature differences exceed 25°C in equatorial latitudes so that the interstitial water could be lighter by 3–4 kg m⁻³.

Our experiments indicate that the buoyant fluid has only a small role to play in the flow dynamics until sufficient sediment has been deposited that the current approaches neutral buoyancy. The experiments also suggest that the effects of buoyancy will then play a role in two regions. First, when the concentration of particles in the current feeding the flow head has been reduced to a few kg m⁻³ the temperature differences will be sufficient to generate lofting in the distal regions. The current would halt leaving a deposit with a fairly abrupt end, and the remaining fine-grained sediment and warmer but more saline water would be mixed into the overlying weakly stratified deep ocean water. Second, the more dilute mixing layer formed over the entire

region of the current would become weakly buoyant and vertical mixing of very fine sediment into the overlying ocean could be expected. The fine sediment from the lofted fluid may become much more widely dispersed than the current deposit to form the pelitic muddy 'e' division of turbidites. We note that the buoyant cloud will spread both away from and towards the source region of the turbidity current and could result in an enhancement in grain size contrast between the 'e' and lower divisions of the Bouma sequence [31], particularly in proximal regions. This process may also contribute to the formation of the nepheloid layer in the few hundred metres above the ocean floor. The experiment in a stratified tank implies that the head and mixing layer could generate plumes of different strength and sediment content, which would create further complexity in the dispersal of fine sediment.

Stow and Wezel [32] have documented fine-grained turbidites from the Bengal fan which have characteristics consistent with deposits from lofted plumes. The units are termed hemiturbidites and are extensively burrowed to depths of several tens of centimetres. Stow and Wezel interpret the burrowing sequences and depths as evidence of unusually slow sedimentation rates of a few millimetres per day, rates so slow that the burrowing organisms can continue their activities. They invoke the mixing of the turbulent upper parts in the distal region of major turbidity currents into the overlying ocean. Their description implicitly invokes the lofting mechanism analysed quantitatively in this paper.

These processes also contribute to vertical mixing and layering within the oceans. Our experimental demonstration of multiple intrusions into a stratified environment show that the interactions between the buoyant fluid liberated from turbidity currents and the oceanic stratification can be quite complex. Wignall and Pickering [33] have observed that faunal diversity increases in sequences of thinly bedded turbidites in the Kimmeridgian sedimentary rocks of Northeast Scotland in comparison to intervening black shale sequences. They attribute the increased faunal diversity to transport of more oxygenated water into the basin by the turbidity current causing turnover of the water column and colonisation. Once sediment supply by turbidity currents ceases

and there is a return to conditions of black shale deposition, mortality occurs. Follmi and Grimm [34] have likewise postulated that burrowing organisms transported from shallow-water environments can survive temporarily in alien deep environments by transport of oxygenated water. The transport of buoyant interstitial water rich in nutrients and oxygen may thus have an important influence on the interpretation of palaeo-environments.

4.2 *Deltaic underflows*

Deltas and estuaries provide an environment where sediment-laden fresh or brackish water is intruded into sea water. When the sediment concentration is sufficiently low, buoyant sediment plumes are dispersed at the ocean surface from which sediment falls out. However in some deltas, such as the Yellow River in China [4], the sediment concentrations can be so high that underflow can form with buoyant interstitial water. Deltas and estuaries are also environments where there are strong lateral density gradients and where storms and strong tidal currents can suspend sediment in sufficient concentrations to initiate gravity currents containing brackish water which flows beneath more saline water.

A good example of such an environment has been documented in the prodelta of the Yellow River. Wright et al. [4] describe a hyperpycnal underflow containing less saline water. This particular current was interpreted to result from suspension of sediment in the brackish delta-top environment by strong parabathymic tidal currents in a storm period rather than by direct entrance of sediment-laden river water. The Yellow River is characterised by very rapid sedimentation in the region of the delta front, and delta progradation can be rapid across this front (1 km in 10 years). Wright et al. [4] documented a substantial decrease in the sedimentation rate in locations only 2 km apart in the downcurrent direction. They attributed the restricted range of sedimentation and underflows to longshore tidal currents. We suggest that underflows are also likely to be curtailed by buoyant lofting and that the rapid decrease in sedimentation rate may alternatively be caused by the intrinsic buoyancy of the currents.

4.3 Co-ignimbrite clouds

The concept of buoyant lift-off has been widely recognised as an explanation for the ash clouds that develop above pyroclastic flows [14,15,35–38] due to a combination of entrainment, thermal expansion and sedimentation. Recent spectacular examples of lift-off occurred in the blast flow of Mt. St. Helens of May 18th 1980 which lofted to form a giant 30 km high cloud [14]. Woods and Kienle [15] describe a co-ignimbrite cloud from the 1990 eruption of Mt. Redoubt in Alaska which formed two separate intrusions at different levels in the atmosphere. They suggested that these two intrusions represented two different events of different strengths and buoyancy. Our experiments in a stratified environment show that it is also possible to generate intrusions at two different levels from a single flow. The more buoyant and less diluted fluid lifting off from the head generates a more powerful upper intrusion, whereas the more diluted and less buoyant fluid lifting off from the mixing layer generates a weaker lower intrusion. Thus, because the density of a pyroclastic flow will similarly vary along its length, the double anvil structure of the Redoubt column may be explicable without invoking two separate events.

Acknowledgements

This research was supported by grants from the British Petroleum Venture Research Unit. Laboratory help in Bristol was provided by Giray Ablay. Comments on an earlier version of the paper by Tim Druitt, Ross Kerr, Takehiro Koyaguchi, Mike Leeder, Nick McCave, Henry Pantin, Kevin Pickering, Colin Wilson and Andy Woods were very much appreciated.

References

- 1 J.E. Simpson, *Gravity Currents in the Environment and the Laboratory*, 244 pp., Halstead Press, 1987.
- 2 D.L. Inman, C.E. Nordstrom and R.E. Flick, Currents in submarine canyons: an air–sea–land interaction, *Annu. Rev. Fluid Mech.* 8, 275–310, 1976.
- 3 P.H. Kuenen and C.I. Migliorini, Turbidity currents as a cause of graded bedding, *J. Geol.* 58, 91–127, 1950.
- 4 L.D. Wright, W.J. Wiseman Jr., Z.S. Yang, B.D. Bornhold, G.H. Keller, D.B. Prior and J.N. Suhayda, Processes of marine dispersal and deposition of suspended silts off the modern mouth of the Juanghe (Yellow) River, *Cont. Shelf Res.* 10, 1–40, 1990.
- 5 C.J.N. Wilson, Pyroclastic flows and ignimbrites, *Sci. Progress Oxford* 70, 171–207, 1986.
- 6 G.V. Middleton, Experiments on density and turbidity currents III: deposition of sediment, *Can. J. Earth Sci.* 4, 475–505, 1967.
- 7 G.V. Middleton and W.J. Neal, Experiments on the thickness of beds deposited by turbidity currents, *J. Sediment. Petrol.* 59, 297–307, 1989.
- 8 G. Parker, Y. Fukushima and H.M. Pantin, Self-accelerating turbidity currents, *J. Fluid Mech.* 171, 145–181, 1986.
- 9 H.M. Pantin, Interaction between velocity and effective density in turbidity flow: phase-plane analysis with criteria for autosuspension, *Mar. Geol.* 31, 59–99, 1979.
- 10 M.W. Stacey and A.J. Bowen, A comparison of an auto-suspension criterion to field observations of five turbidity currents, *Sedimentology* 37, 1–5, 1990.
- 11 G.V. Middleton, Experiments on density and turbidity currents. III. Deposition of sediment, *Can. J. Earth Sci.* 4, 475–505, 1967.
- 12 J.R.L. Allen, The Bouma Division A and the possible duration of turbidity currents, *J. Sediment. Petrol.* 61, 291–295, 1991.
- 13 R.P. Denlinger, A model for generation of ash clouds by pyroclastic flows, with application to the 1980 eruptions of Mount St. Helens, Washington, *J. Geophys. Res.* 92, 10284–10298, 1987.
- 14 R.S.J. Sparks, C.J. Rice and J.G. Moore, The giant eruption cloud of the May 18th, 1980, explosive eruption of Mount St. Helens, *J. Volcanol. Geotherm. Res.* 28, 257–274, 1986.
- 15 A.W. Woods and J. Kienle, The dynamics and thermodynamics of volcanic clouds: Theory and observations from the April 15 and April 21, 1990 eruptions of Redoubt, Alaska, *J. Volcanol. Geotherm. Res.*, in press.
- 16 S.N. Carey, H. Sigurdsson and R.S.J. Sparks, The fluid dynamic behaviour of particle-laden plumes, *J. Geophys. Res.* 93, 15314–15328, 1988.
- 17 D. Quadfasel, H. Kudrass and A. Frische, Deep-water renewal by turbidity currents in the Sulu Sea, *Nature* 348, 320–322, 1990.
- 18 H.E. Huppert, R.C. Kerr, J.R. Lister and J.S. Turner, Convection and particle entrainment driven by differential sedimentation, *J. Fluid Mech.* 226, 349–369, 1991.
- 19 R.C. Kerr, Erosion of a stable density gradient by sedimentation-driven convection, *Nature* 353, 423–425, 1991.
- 20 T. Koyaguchi, M.A. Hallworth, H.E. Huppert and R.S.J. Sparks, Sedimentation of particles from a convecting fluid, *Nature* 343, 447–450, 1990.
- 21 R.C. Kerr and J.R. Lister, Further results for convection driven by the differential sedimentation of particles, *J. Fluid Mech.* 243, 227–245, 1992.
- 22 H. Rouse, ed., *Engineering Hydraulics*, pp. 763–765, Wiley, New York, 1950.
- 23 D. Martin and R. Nokes, Crystal settling in a vigorously convecting magma chamber, *Nature* 332, 534–536, 1988.
- 24 R.S.J. Sparks, S.N. Carey and H. Sigurdsson, Sedimenta-

- tion from gravity currents generated by turbulent plumes, *Sedimentology* 38, 839–856, 1991.
- 25 H.A. Einstein, Deposition of suspended particles in a gravel bed, *J. Hydraul. Div., Am. Soc. Civ. Eng.* 92, 1197–1205, 1968.
 - 26 I.N. McCave, Deposition of fine grained suspended sediment from tidal currents, *J. Geophys. Res.* 75, 4151–4159, 1970.
 - 27 H.E. Huppert and J.E. Simpson, The slumping of gravity currents, *J. Fluid Mech.* 99, 785–799, 1980.
 - 28 R.T. Bonnecaze, H.E. Huppert and J.R. Lister, Sediment-driven gravity currents, *J. Fluid Mech.*, in press.
 - 29 T.K. Fannelop and G.D. Waldman, Dynamics of oil slicks, *AIAA J.* 10, 506–510, 1972.
 - 30 D.P. Hoult, Oil spreading on the sea, *Annu. Rev. Fluid Mech.* 4, 341–368, 1972.
 - 31 A.H. Bouma, *Sedimentology of some Flysch Deposits*, Elsevier, Amsterdam, 1962.
 - 32 D.A.V. Stow and A. Wetzell, Hemiturbidite: a new type of deep water sediment, *Proc. ODP* 116, 25–34, 1990.
 - 33 P.B. Wignall and K.T. Pickering, Fault-controlled sedimentation in the Kimmeridgian (Late Jurassic) of N.E. Scotland, *J. Geol. Soc. London*, in press.
 - 34 K.B. Follmi and K.A. Grimm, Doomed pioneers: gravity flow and bioturbation in marine oxygen-depleted environments, *Geology* 18, 1069–1072, 1990.
 - 35 A. Lacroix, *La Montagne Pelée et ses éruptions*, 662 pp., Masson et Cie, Paris, 1904.
 - 36 T. Anderson and J.S. Flett, Report on the eruptions of the Soufrière in St. Vincent and a visit to Montagne Pelée in Martinique, Pt. I, *R. Soc. London Philos. Trans. Ser. A*, 200, 353–553, 1903.
 - 37 R.S.J. Sparks and G.P.L. Walker, The significance of vitric-enriched air-fall ashes associated with crystal-enriched ignimbrites, *J. Volcanol. Geotherm. Res.* 2, 329–341, 1977.
 - 38 A.W. Woods and K. Wohletz, Dimensions and dynamics of co-ignimbrite eruption columns, *Nature* 350, 225–227, 1991.